Anaerobic oxidation of methane in sediments of a nitrate-rich, oligo-mesotrophic boreal lake

Antti J Rissanen[1,*], Tom Jilbert[2], Asko Simojoki[3], Rahul Mangayil[1], Sanni L Aalto[4,5,a], Sari Peura[6], Helena Jäntti[4]

[1]Faculty of Engineering and Natural Sciences, Tampere University, Korkeakoulunkatu 6, FI-33720, Tampere, Finland

[2]Ecosystems and Environment Research Program, Faculty of Biological and Environmental Sciences, University of Helsinki, P.O. Box 65, FI-00014, Helsinki, Finland

[3]Department of Agricultural Sciences (Environmental Soil Science), Faculty of Agriculture and Forestry, University of Helsinki, P.O. Box 56, FI-00014, Helsinki, Finland

[4]Department of Environmental and Biological Sciences, University of Eastern Finland, Yliopistonranta 1 E, FI-70210, Kuopio, Finland

[5]Department of Biological and Environmental Sciences, University of Jyväskylä, Survontie 9 C, FI-40014, Jyväskylä, Finland

[6]Department of Forest Mycology and Plant Pathology, Science for Life Laboratory, Swedish University of Agricultural Sciences, Almas allé 5, SE-75651, Uppsala, Sweden

[a]Current address: Technical University of Denmark, DTU Aqua, Section for Aquaculture, The North Sea Research Centre, P.O. Box 101, DK-9850, Hirtshals, Denmark

*Corresponding author: Antti J Rissanen, Faculty of Engineering and Natural Sciences, Tampere University, Korkeakoulunkatu 6, FI-33720, Tampere, Finland. Tel: +358 40 1981145; Fax: +358 3 3641392; e-mail: antti.rissanen@tuni.fi

Abstract

The identity of electron acceptors in promoting anaerobic oxidation of methane (AOM) in the sediments of boreal lakes is currently unknown. Here, we studied the AOM rate of sediment slurries collected from three profundal stations of a nitrate-rich, oligo-mesotrophic, boreal lake (Lake Pääjärvi, Finland), under varying nitrate concentrations using ^{13}C-labelling. Furthermore, vertical profiles of the sediment and porewater geochemistry, and the microbial communities (16S rRNA gene and shotgun metagenomic sequencing) were analyzed. Despite geochemical data indicating that simultaneous consumption of nitrate and methane took place at the sediment layers chosen for incubations, AOM rate was not enhanced by nitrate amendments at either of the stations. AOM rate was much higher at the shallow Station 1 (0.9-6.8 nmol C cm^{-3} d^{-1}) with high contents of labile phytoplankton-derived organic matter, than at the deeper stations, Station 2 (0-0.3 nmol C cm^{-3} d^{-1}) and 3 (0-0.2 nmol C cm^{-3} d^{-1}). Accordingly, a higher relative abundance of methanotrophic archaea (*Candidatus* Methanoperedens) and bacteria (*Methylococcales*) were observed in the layers chosen for incubations at Station 1 than at the other stations. Besides nitrate, the geochemical profiles indicated that AOM was potentially coupled with iron or sulfate reduction at all stations. Furthermore, putative nitrite-reducing methanotrophs (*Ca*. Methylomirabilis) were the most abundant methanotrophs above the incubation layer at Station 2 and 3, which suggests that nitrite reduction also plays a role in driving AOM in the study lake. We conclude that AOM is not uniquely coupled to nitrate reduction in sediments of nitrate-rich, oligo-mesotrophic, boreal lakes.

Keywords: anaerobic oxidation of methane, nitrate, lake, methanotroph, shotgun metagenomics, 16S rRNA gene

Introduction

The concentration of atmospheric methane (CH_4), a critical greenhouse gas, has increased substantially since industrialization, with current total emissions 550 – 600 Tg/year (top-down estimates by Saunois et al. 2020). Roughly 40 % of these emissions stem from natural sources (Saunois et al. 2020), mostly produced by archaea through methanogenesis. Lakes are important natural emitters of CH_4 (Bastviken et al. 2011). The numerous lakes and ponds in the northern boreal zone with annual emissions of ~16.5 Tg are especially significant contributors to the global CH_4 budget (Wik et al. 2016). Thus, knowledge on the factors affecting CH_4 emissions from northern lakes is essential for accurate estimates and modelling of global CH_4 budget.

Besides methanogenesis, microbial oxidation of CH_4 taking place in sediments and water columns is an important controller of the CH_4 emissions from lake ecosystems (Deutzmann et al. 2014). A recent study has reported that the anaerobic oxidation of methane (AOM) consumes large proportions (12 – 87 %) of gross CH_4 production in sediments of some boreal lakes (Martinez-Cruz et al. 2018). Nevertheless, contrasting observations (i.e. negligible role of AOM in reducing CH_4 emissions) from other boreal lakes have been also reported (Rissanen et al. 2017; Kallistova et al. 2018). This discrepancy can be due to varying availabilities of AOM-driving electron acceptors (EAs, i.e. NO_3^-, NO_2^-, Fe^{3+}, Mn^{4+}, SO_4^{2-} and organic EAs) between lakes. However, the identity of EAs driving AOM in lake sediments is understudied and such data is especially scarce from boreal lakes (Rissanen et al. 2017; Kallistova et al. 2018; Martinez-Cruz et al. 2018). The quality of EAs driving AOM in natural ecosystems is usually studied in experimental incubations, where AOM rates are measured at increased concentration levels of EAs (Beal et al. 2009; Rissanen et al. 2017). In the few previous studies of boreal lake sediments, additions of Fe^{3+}, Mn^{4+}, SO_4^{2-} or NO_3^- did not enhance AOM (Rissanen et al. 2017;

Kallistova et al. 2018). This was despite the fact that the sediments harbored typical freshwater AOM organisms, i.e. archaea in genus *Ca*. Methanoperedens sp. (also known as ANME-2D archaea), that potentially use a wide variety of EAs (e.g. NO_3^-, Fe^{3+}, Mn^{4+} and SO_4^{2-}), and bacteria of genus *Ca*. Methylomirabilis sp. (within phylum *NC10*), that use NO_2^- (Ettwig et al. 2010, 2016; Haroon et al. 2013; Weber et al. 2017; Rissanen et al. 2017). Previously, NO_3^-/NO_2^- was shown to drive AOM in sediments of a eutrophic NO_3^- - rich lake and a pond in temperate area (Norði and Thamdrup 2014; Deutzmann et al. 2014). However, such data do not exist from NO_3^- - rich boreal lakes.

To shed light on the identity of EAs driving AOM in boreal lakes, we studied the effect of NO_3^- additions on AOM in sediments of a NO_3^- - rich boreal lake, Lake Pääjärvi (Southern Finland). This was complemented with analyses of vertical profiles of sediment and porewater geochemistry, and the associated microbial communities were studied using 16S rRNA gene sequencing and shotgun metagenomics. We hypothesized that due to the high availability of NO_3^-, AOM is linked to NO_3^- reduction, and, thus, NO_3^- addition enhances AOM in the sediments of the studied lake.

Materials and methods

Study lake

Lake Pääjärvi is a NO_3^- - rich, oligo-mesotrophic lake in southern Finland (61.04N, 25.08E; A = 13.4 km^2, max. depth = 87 m, mean residence time = 3.3 years). The water column circulates twice per year and is always well oxygenated (Salonen 1981). The large catchment area of Lake Pääjärvi (244 km^2) is dominated by forests and agriculture. Since the 1970s, the nutrient concentrations of the water have increased (Arvola et al. 1996).

Porewater and sediment sampling

Vertical profiles of the porewater and sediment samples were collected from three stations in Lake Pääjärvi on 9th August 2017 using a hand-held HTH/Kajak corer with plexiglass tubes (Table 1). The stations followed a water depth gradient, Station 1 being shallowest and Station 3 deepest (Table 1). The core tubes were pre-drilled with two vertical series of 4 mm holes (each at 2 cm resolution), then taped, in preparation for porewater sampling with Rhizons™ (Rhizosphere research products, Wageningen, Netherlands). Rhizon sampling automatically filters the porewaters at 0.15 µm into attached 10 ml syringes under vacuum. One vertical series of samples was taken for analysis of dissolved CH_4 and dissolved inorganic carbon (DIC). The syringes were pre-filled with 1 ml of 0.1M HNO_3 to immediately convert all DIC to CO_2. A known volume of N_2 gas headspace was injected into the syringes after sampling, and the samples were shaken to equilibrate the dissolved gases with the headspace. The subsamples of the headspace were then extracted into 3 mL Exetainers™ (Labco Limited, Lampeter, UK) and stored at room temperature until analysis (for full details see Jilbert et al. 2020). The second vertical series was taken for analyses of S, Fe, and P [by inductively coupled plasma atomic emission spectroscopy (ICP-OES)], NO_3^-, and organic fermentation products. Subsamples for analyses of NO_3^- and fermentation products were stored frozen at -20 °C until analysis. The subsamples for ICP-OES were acidified with 1 M HNO_3 and stored at room temperature. After porewater sampling, the sediment cores were sliced into plastic bags at a resolution of 1 cm or 2 cm at 0–10 cm or >10 cm depth below the surface of sediment, respectively. The subsamples of 400 – 500 µl wet sediment were collected from the depth of 0–10 cm at each station and stored frozen at -20 °C for DNA-based molecular microbiological analyses. The remaining wet sediment samples were stored frozen at -20 °C under N_2 until further processing.

Porewater and sediment bulk geochemical analysis

According to our standard protocols, all the Rhizon samples were sequentially washed with 0.01 M HNO_3 and MilliQ water before field sampling. Later, it was noticed that the washing procedure caused background contamination in the porewater NO_3^- measurements. The magnitude and variability of this contamination was tested by sampling a solution of MilliQ water through the Rhizon samplers in plastic syringes and determining the NO_3^- concentration of the extracted sample. The same procedure was repeated using both factory-clean (9 replicates) and 0.01M HNO_3-washed Rhizons (10 replicates). The difference between the mean NO_3^- values, determined from the factory-clean and washed Rhizon samples (30.0 µmol L^{-1}), was subtracted from all the porewater NO_3^- data of this study. For objectivity, we report here the corrected values, as well as the error margins representing the full range of observed contamination (min – max, 16.8 µmol L^{-1} – 73.9 µmol L^{-1}). The porewater nitrate concentrations were determined according to Miranda et al. (2001), while the samples from the HNO_3 – contamination test were analyzed by QuikChem®8000 flow injection analyzer (Lachat Instruments, Hach Co., Loveland, CO, USA) according to Wood et al. (1967).

The S, Fe and P concentrations in the porewater samples were determined by ICP-OES (Thermo iCAP 6000, Thermo Fisher Scientific, Waltham, MA, USA). In this system, S is expected to be dominated by sulfate (SO_4^{2-}), Fe by Fe^{2+}, and P by orthophosphate ($H_2PO_4^-$), although in each case, other forms are possible. The porewater CH_4 and DIC concentrations were determined by gas chromatography (GC) as described in Jilbert et al. (2020). Briefly, the sample vials (Exetainers) were pressurized with helium (He) to 2.0 bar before loading into the GC (Agilent technologies 7890B GC system, Agilent Technologies, Santa Clara, Ca, USA). CH_4 was determined by flame-ionization detector (FID) and CO_2 by thermal conductivity detector (TCD).

The instrument simultaneously measures N_2 and O_2 + Ar (in TCD), from which a 100% sum can be calculated for estimation of CH_4 and CO_2 concentrations in the original sample, in ppm by volume. For a full description of the calculations, see Jilbert et al. (2020).

Sediment samples were freeze-dried, ground in an agate mortar and weighed into tin cups for carbon (C) and nitrogen (N) content determinations. In accordance with extensive previous studies on Finnish lake sediments (Pajunen 2000; Kortelainen et al. 2004), acidification was not applied prior to the determinations. High levels of organic acidity from Finnish river catchments (Kortelainen and Saukkonen 1995) maintain low annual mean pH values in most lakes and therefore there is negligible occurrence of carbonates in lake sediments. Hence our total C data is considered equivalent to organic C (C_{org}). C and N contents were determined using elemental analyzer (LECO TruSpec Micro, LECO Corp., St. Joseph, MI, USA).

Organic fermentation products in porewaters were analyzed using high performance liquid chromatography (HPLC) equipped with Shodex SUGAR column (300 mm × 8 mm, Phenomenex, Torrance, CA, USA), autosampler (SIL-20AC HT, Shimadzu, Kioto, Japan), refractive index detector (RID-10A, Shimadzu), and 0.01 M H_2SO_4 as the mobile phase. The HPLC samples were prepared as described in Salmela et al. (2018). The identification and quantification of the liquid metabolites (lactate, acetate and propionate) were conducted using external standards.

Incubations for the AOM measurements

The sediment for the incubation experiments was collected from the same three stations, one week after the collection of porewater and sediment samples (15th Aug 2017), using plexiglass tubes (diameter = 7 cm) connected to a gravity corer (Table 1). The initial porewater profile data

were used to select the optimum depth horizons for sampling sediments for the incubations. At each station, a 3 cm thick sediment slice was cut immediately below the layer at which the porewater Fe concentrations started to increase downwards, indicating the onset of anaerobic remineralization processes and therefore a suitable depth interval for the incubation experiments. The upper limits to the incubation slices are as follows: -1 cm at Station 1 (thus, layer 1 – 4 cm from surface); -3 cm at Station 2 (layer 3 – 6 cm) and -3 cm at Station 3 (layer 3 – 6 cm).

The sediment from each station was mixed in 1:1 ratio with filtered (0.6 µm glass fiber filter) water collected 50 cm above the sediment. The sediment slurry was prepared in a 1 L bottle and purged with N_2 for 10 min. Thereafter, the bottle was quickly capped with a septum and the headspace was purged again with N_2 for 5 min. To ensure anoxic conditions prior to the experiments, the bottle containing the sediment slurry was placed on a shaker table overnight at 5°C and 120 rpm to facilitate the removal of any residual O_2. Thereafter, the set-up of incubations was conducted in a glove bag with N_2 atmosphere. The sediment slurry was transferred into 12 ml glass vials (Exetainers) (2 ml of slurry per vial), after which the vials were filled with filtered (0.6 µm), anoxic, N_2-purged bottom water. Thereafter, sterile, anoxic, N_2-purged stock solution of KNO_3 was added to the vials in concentrations of 0, 10, 50, 100, 200 and 500 µmol (N) L^{-1}. There were 57 vials altogether: i.e. three vials per each NO_3^- concentration at each station (3 stations x 6 concentrations x 3 vials = 54) and, furthermore, one vial at each station represented a non-incubated control sample (without KNO_3) of the slurry at the beginning of the experiment (= 3). The vials were capped with septum, followed by the addition of 100 µl of gaseous ^{13}C-labeled CH_4 (^{13}C = 99.9%, Cambridge Isotope Laboratories Inc., Tewksbury, MA, USA) into two vials per each NO_3^- concentration at each station. One vial per each NO_3^- concentration at each station was not amended with ^{13}C-CH_4 and hence was included as a non-

labeled incubation control. The vials were taken out of the glove bag, shaken for 3 minutes to aid the dissolution of the added methane and incubated on a shaker (120 rpm) at 5 °C in the dark for 21.7, 20.75 and 20.25 hours for Station 1, 2 and 3, respectively.

After incubations, 3 ml of slurry per sample were injected into pre-evacuated He-filled 12 ml vials (Exetainers) (over-pressure was released from the He-filled vials before sampling), which contained 300 µL of H_3PO_4 (85%) to ensure the transformation of DIC into CO_2. The samples were then stored inverted at +4 °C until the analysis.

Stable isotopic and concentration analyses of DIC

Stable isotopic and concentration analyses of DIC were performed using an Isoprime100 isotope ratio mass spectrometer (IRMS) (Elementar UK Ltd., Cheadle, UK) coupled to an Isoprime TraceGas pre-concentration unit. The isotopic data was calculated as the fractional abundance of ^{13}C, i.e. ^{13}F, in DIC, using equation 1.

$$^{13}F = \frac{^{13}C}{(^{13}C + ^{12}C)} \quad (1)$$

Calculations

A simple two-component mixing model was applied for a first-order quantification of the relative contributions of terrestrial plant-derived and autochtonous phytoplankton-derived organic matter to the total sedimentary organic matter (% of total organic C). The calculation uses the molar N:C ratio of organic matter, and end-member values, N/C_{EM}, based on the studies of Goñi et al. (2003) and Jilbert et al. (2018):

$$\%OC_{phyt} = \frac{\left(N/C_{sample} - N/C_{EM-terr}\right)}{\left(N/C_{EM-phyt} - N/C_{EM-terr}\right)} \times 100 \quad (2)$$

$$\%OC_{terr} = 100 - \%OC_{phyt} \quad (3)$$

where $N/C_{EM\text{-}terr} = 0.04$, and $N/C_{EM\text{-}phyt} = 0.13$. The calculation assumes that terrestrial plant matter and phytoplankton are the only sources of organic material present in the samples, the N/C values are spatially and temporally fixed at the end-member values, and the values do not alter significantly during sedimentation and burial of organic matter.

AOM rates were determined from the production rate of excess ^{13}C-labeled DIC,

$$\text{Excess } ^{13}\text{C-DIC} = (^{13}F_L - {}^{13}F_n) \times C_{conc} \quad (4)$$

where C_{conc} is the concentration of DIC, and $^{13}F_L$ is the fractional abundance of ^{13}C in ^{13}C-labeled samples, while $^{13}F_n$ denotes that in non-labeled samples (see equation 1). Assuming that the excess ^{13}C-DIC was zero at the beginning, we used a single time point measurement, i.e. excess ^{13}C-DIC after the incubations, to determine the AOM rate, expressed as a rate per dry weight (DW) or per volume of sediment per hour (nmol C g^{-1}_{DW} h^{-1} or nmol C cm^{-3} h^{-1}). The added amount of CH_4 (i.e. 100 µl, see above) corresponds to a concentration of approximately 320 µmol L^{-1}, which is on average 8 – 14 times higher than the natural CH_4 concentration in the depth layers chosen for the incubations (see Results and Discussion). Furthermore, considering that the slurry preparations led to only 1 mL of the original sediment to be added to each vial (i.e. 2 mL of 1:1 water:sediment – slurry added to each 12 mL vial, which was then filled with water, see above), the added ^{13}C-labeled CH_4 was estimated to account of almost all (> 99 %) of CH_4 in the incubation vial. Thus, the measured production rates of excess ^{13}C-DIC represent AOM rates. The CH_4 oxidation in this study was determined solely based on the transfer of ^{13}C from CH_4 to

DIC, and hence, the proportion of CH_4-C bound to the biomass or extracellular organic metabolites was not taken into account.

DNA extraction

DNA was extracted from the frozen sediment samples using DNeasy PowerSoil Kit (Qiagen, Hilden, Germany). DNA concentration was measured using a Qubit 2.0 Fluorometer and a dsDNA HS Assay Kit (Thermo Fisher Scientific, Waltham, MA, USA).

16S rRNA gene amplicon sequencing

PCR and 16S rRNA gene amplicon sequencing was performed by The Foundation for the Promotion of Health and Biomedical Research of Valencia Region (FISABIO, Valencia, Spain). In the PCR reactions, the V4 region of the bacterial and archaeal 16S rRNA genes were simultaneously targeted using primer pair 515FB (5'-GTGYCAGCMGCCGCGGTAA-3´)/806FB (5'-GGACTACNVGGGTWTCTAAT-3´) (Apprill et al. 2015; Parada et al. 2016) . PCR, library preparation and sequencing (Illumina MiSeq, Illumina, San Diego, CA, USA) was performed as previously described (Myllykangas et al. 2020), except that, in PCR reactions, approximately 15 ng of DNA were used.

Shotgun metagenomic sequencing

The shotgun metagenomic sequencing was performed by Novogene Co.,Ltd (Hong Kong). The libraries were prepared from ~100 ng of DNA per sample using the NEBNext® Ultra™ DNA Library Prep Kit for Illumina® (New England Biolabs, Ipswich, MA, USA) according to the

manufacturer´s protocol. The sequencing was done on Illumina HiSeq X Ten System (Illumina) with paired-end mode and 150 bp read length producing from ~9 to ~12 Gb of raw data per sample.

Bioinformatic analyses of 16S rRNA gene data

The quality assessment of the raw sequence reads, merging of paired end reads, alignment, chimera removal, preclustering, taxonomic classification (and removal of chloroplast, mitochondria, and eukaryote sequences) and division of 16S rRNA gene sequences into operational taxonomic units (OTUs) at 97 % similarity level was conducted as previously described (Rissanen et al. 2020). Singleton OTUs (OTUs with only 1 sequence) were removed, and the data were then normalized by subsampling to the same size, 77340 sequences. One sample, representing the layer 8-9 cm depth at Station 3, was discarded from the analyses since it had only ~10 000 sequences.

Bioinformatic analysis of shotgun metagenomic data

The raw sequences were analyzed using The European Bioinformatics Institute (EBI) Metagenomics pipeline (version 4.1) for trimming and taxonomic analysis of the reads containing 16S rRNA gene sequences against Silva 132 database (Mitchell et al. 2017). Furthermore, Kaiju web server (http://kaiju.binf.ku.dk/server) was used for taxonomic classification of the raw reads against National Center for Biotechnology Information´s (NCBI) nr – database (Menzel et al. 2016).

For metagenomic binning analysis, the raw data was trimmed using Trimmomatic (version 0.39) (Bolger et al. 2014). The trimmed data was assembled using Megahit (version 1.2.8) (Li et al.

2015). The quality-controlled reads were mapped to the assembly using BBmap (version 38.73) (https://sourceforge.net/projects/bbmap/). The mapping results were used to bin the contigs using Metabat2 (Kang et al. 2015, 2019). The genes of the obtained metagenomic bins were predicted and annotated using Prokka (version 1.14.5) (Seemann 2014). The bins were also taxonomically annotated using CAT/BAT – tool and NCBI´s nr – database and taxonomy (von Meijenfeldt et al. 2019). Prokaryotic completeness and redundancy were computed using CheckM (version v1.1.2) (Parks et al. 2015). Taxonomic annotations were specifically screened for bins affiliated to known aerobic (gamma- and alphaproteobacterial MOBs) and anaerobic methanotrophs (ANME archaea and *Ca*. Methylomirabilis sp. bacteria). Furthermore, functional annotations were specifically screened for bins coding for particulate and soluble methane mono-oxygenases, key enzymes in aerobic methanotrophy and in *Ca*. Methylomirabilis sp. – mediated AOM, and for methyl coenzyme M reductase, the key enzyme in methanogenesis and in ANME archaea - mediated AOM.

Statistical analyses

The variation between stations and between NO_3^- concentrations was studied using a two-way analysis of variance (2-ANOVA) with station (3 levels) and NO_3^- concentration (6 levels) as fixed factors followed by pair-wise post hoc tests using least significant difference (LSD) technique with Hochberg-Bonferroni corrected α-values. The relationship between the varying NO_3^- concentration and AOM was also studied specifically at each station using Spearman correlation analysis.

In addition, the variation between stations in relative abundance of different methanotrophic, methanogenic and SO_4^{2-} reducing taxa at the depth layers representing the AOM incubation depths was analyzed using randomized block analysis of variance (RB-ANOVA) with the depth

layer (three 1 cm layers at each station) as the blocking factor. RB-ANOVA was followed by pair-wise post-hoc tests using LSD technique with Hochberg-Bonferroni-corrected α-values. Furthermore, the coherence in the depth patterns between ANME archaea and SO_4^{2-} reducing bacteria was analyzed by Spearman correlation analysis. All the analyses were done using IBM SPSS Statistics 26 (IBM SPSS Statistics for Windows, Version 26.0, IBM Corp., Armonk, NY, USA).

Sequence database accession

The sequences of the 16S rRNA gene amplicon dataset are deposited in NCBI´s Sequence Read Archive (SRA) under the accession number PRJNA627335. The sequences of the shotgun metagenomic dataset are deposited in European Nucleotide Archive (ENA) under the accession number PRJEB29513.

Results and discussion

Sediment chemical characteristics and the structure of the methanogenic community

All the stations showed a broadly similar diagenetic zonation based on the porewater chemistry (Figs. 1 and 2). The vertical profiles of porewater concentrations of NO_3^-, S (assumed to be mostly SO_4^{2-}), Fe (assumed to be mostly Fe^{2+} from reduction of solid-phase Fe oxides) and CH_4 suggest a transition zone, wherein the upwards-diffusing CH_4 is oxidized by anaerobic respiration linked to reduction of NO_3^-, SO_4^{2-}, and Fe oxides. This zone was slightly closer to the sediment surface at Station 1 than at the other stations (Figs. 1 and 2). Station 1 also had higher

overall concentrations of CH_4 and CO_2 than Station 2 and 3, and was the only station where lactate was observed in the porewaters (Fig. 2). In addition, while acetate and propionate were observed at all stations, they were at slightly higher concentrations at Station 1 than at the other two stations (Fig. 2). These results suggest that there was lower redox-potential and higher degree of fermentation at Station 1, which very likely led to higher rates of production of fermentation products and methanogenesis. This may be due to higher lability of organic matter, being supported by our estimates on the contribution (%) of phytoplankton-derived organic carbon, which was slightly higher at Station 1 than at Station 2 and 3 (Fig. 2).

In accordance with lower redox-potential and higher rates of methanogenesis at Station 1, the relative abundance of methanogens [shown as average % (min-max) of 16S rRNA gene amplicons] in the studied layer (topmost 10 cm) was generally higher there [0.5 % (0.01-1.1 %)] than at Station 2 [0.3 % (0.006-1.8 %)] and 3 [0.1 % (0.003-0.5 %)] (Fig. 3). The order *Methanomassiliicoccales*, whose cultivated members drive solely the methyl reducing methanogenic pathway (Borrel et al. 2013), dominated the methanogen communities at all stations (Fig. 3). Nevertheless, the hydrogenotrophic (i.e. H_2-consuming) CO_2 reducing methanogens of the order *Methanomicrobiales* (Nazaries et al. 2013) made also a significant proportion of methanogenic community at Station 1 but not at the other two stations (Fig. 3). The dominance of *Methanomassiliicoccales* is surprising, because methanogenesis in freshwater sediments is typically dominated by the acetoclastic (i.e. acetate – utilizing) and hydrogenotrophic CO_2 reducing pathways (Conrad 1999). However, a recent metagenomic data suggested the presence of the acetoclastic pathway in genomes of uncultivated *Methanomassiliicoccales*, which could explain our findings (Speth and Orphan 2018). On the other hand, being only very recently described order with currently limited information on its

functional diversity (Iino et al. 2013), *Methanomassiliicoccales* might also contain species without capability for methanogenesis. Unfortunately, we could not construct metagenome-assembled genomes (MAGs) of *Methanomassiliicoccales* or any other methanogens, probably because they had too low abundance to be detected by the metagenomic binning analysis (see Supplementary Results and Table S1). Hence, the potential functions of *Methanomassiliicoccales* in sediments of the study lake remain uncharacterized.

AOM rates in the sediment

The effect of NO_3^- addition on AOM rates in sediment slurries consisting of layer 1 – 4 cm (from surface) at Station 1 and layer 3 – 6 cm at Station 2 and 3 was analyzed by anaerobic incubations using ^{13}C-labeled CH_4. The complete pore water profiles show that the incubated layers of each core were suitably chosen at the transition between high NO_3^- and S concentrations (above) and high Fe^{2+} and CH_4 concentrations (below), indicating the zone of active reduction of NO_3^-, SO_4^{2-} and Fe^{3+} and consumption of CH_4 (Figs. 1-3).

In comparison to non-labelled control samples, incubation with amendments of ^{13}C-labeled CH_4 led to ^{13}C-enrichment of DIC. The ^{13}C-enrichment of DIC was much higher at Station 1 than at Station 2 and 3 (Fig. S1). In accordance, the AOM rates were significantly higher at Station 1 (min-max: 0.3 – 1.8 nmol C g^{-1}_{DW} h^{-1}) than at Station 2 (0 – 0.07 nmol C g^{-1}_{DW} h^{-1}) or 3 (0 – 0.06 nmol C g^{-1}_{DW} h^{-1}) (2-ANOVA, $F_{Station} = 45$, $p < 0.001$) (Fig. 4). The AOM rates (converted to volumetric rates, 0 – 6.8 nmol C cm^{-3} d^{-1}) are within the lower end of AOM rates reported from lake sediments in general (0 – 180 nmol C cm^{-3} d^{-1}) and from boreal lakes in particular (0 – 16.3 nmol C cm^{-3} d^{-1}) (Deutzmann and Schink 2011; Rissanen et al. 2017; Martinez-Cruz et al. 2018). However, the AOM rates at Station 1 (0.9 – 6.8 nmol C cm^{-3} d^{-1}) correspond well with the

median AOM (3.5 nmol C cm^{-3} d^{-1}) of the multiple lake studies reviewed by Martinez-Cruz et al. (2018).

In agreement with both insignificant rank correlation ($p > 0.05$) and 2-ANOVA analyses ($F_{concentration} = 0.7$, $p > 0.05$), increasing concentration of NO_3^- did not enhance AOM at any of the stations (Fig. 4). Hence, despite the evidence from the geochemical profiles, these results suggest that AOM was not directly coupled with NO_3^- reduction in the sediments of the study lake. We acknowledge that the tested nitrate concentration levels (sum of added nitrate and nitrate already present in the slurry) were on average 7-57, 5-35 and 1-13 times higher than that naturally present in the incubation layers at Station 1, 2 and 3, respectively (Figs. 3 and 4). However, we find it unlikely that the observed independence between nitrate concentration and AOM would be caused by nitrate-saturation of AOM at high nitrate concentrations. This is because the fact that also the added ^{13}C-CH_4 concentrations were much higher, on average 9, 14 and 8 times higher, than natural CH_4 concentrations at Station 1, 2 and 3, respectively. Hence, instead of NO_3^-, AOM appears to be coupled with reduction of other EAs, e.g. Fe^{3+} or SO_4^{2-}, as suggested by the geochemical profiles, or organic EAs (Valenzuela et al. 2017; Su et al. 2019). Furthermore, under SO_4^{2-} - starved conditions, Fe^{3+} reduction can also indirectly support SO_4^{2-} -mediated AOM through oxidation of reduced sulfur species to SO_4^{2-} (Su et al. 2019).

Methanotrophic community in the sediments

Aerobic MOBs, in order *Methylococcales*, as well as anaerobic methanotrophs, in genera *Ca*. Methanoperedens sp. (also known as ANME 2D archaea) and *Ca*. Methylomirabilis sp. (within bacterial phylum *NC10*), were the most abundant groups of methanotrophs present in the studied sediments, agreeing with a previous study on boreal lake sediments (Rissanen et al. 2017) (Figs. 3 and 5). Aerobic MOBs in the family *Methylacidiphilaceae* were rare, while

alphaproteobacterial MOBs were not detected. As expected for aerobic bacteria, the relative abundance of *Methylococcales* methanotrophs was highest at the surface sediment layers and decreased towards deeper layers (Fig. 3). In contrast, *Ca*. Methanoperedens sp. had peaks in its relative abundance at deeper layers clearly below the sediment surface (Fig. 3). *Ca*. Methylomirabilis sp. peaked in its relative abundance both at the surface as well as at deeper sediment layers at all stations (Fig. 3).

Methanotroph communities in the depth layers representing the layers chosen for AOM incubation were specifically compared between stations. As the results of amplicon sequence analyses can be affected by PCR-based biases (e.g. primer bias), these comparisons were also made using PCR-free shotgun metagenomic techniques. *Ca*. Methanoperedens sp. and *Methylococcales* had higher relative abundances at Station 1 than at other stations (Fig. 5), which validates the higher AOM rates obtained from Station 1 (Fig. 4). In contrast, the relative abundance of *Ca*. Methylomirabilis did not vary between the stations (Fig. 5). We acknowledge that these comparisons are based on relative abundances and we lack analyses of absolute abundances (e.g. by quantitative PCR). However, we can assume that the relative abundance of a certain taxa, when expressed as the number of shotgun metagenomic reads relative to all sequenced reads, represents a proxy for the proportion of DNA of the taxa in the total extracted DNA (Fig. 5D). As concentration of DNA in the sediment (average ± SD of three layer specific samples), i.e. 1040 ± 290 ng cm^{-3}, 1170 ± 470 ng cm^{-3} and 870 ± 100 ng cm^{-3} at Station 1, 2 and 3, respectively, did not differ between the stations (RB-ANOVA, $F = 0.5$ and $p > 0.05$), the variations in the relative abundances expressed as number of reads relative to all sequenced reads suggests that also the absolute abundance of *Ca*. Methanoperedens and *Methylococcales* was higher at Station 1 than at the other two stations (Fig. 5D).

In addition to using NO_3^- , *Ca*. Methanoperedens sp. archaea have been suggested to use a wide variety of other EAs in AOM, i.e. SO_4^{2-}, Fe^{3+} and organic compounds (Knittel and Boetius 2009; Ettwig et al. 2016; Timmers et al. 2017; Weber et al. 2017; Bai et al. 2019; Su et al. 2019). Hence, their higher abundance further supports the finding of higher AOM rates at Station 1, potentially coupled with reduction of other EAs than NO_3^-. In addition, ANME archaea drive SO_4^{2-} - dependent AOM usually in syntrophic relationship with SO_4^{2-} reducing bacterial partners (Knittel and Boetius 2009). The relative abundance of SO_4^{2-} reducing bacteria in the depth layers representing the AOM incubation layers did not vary between the stations (Fig. S2A). However, the vertical depth patterns of *Ca*. Methanoperedens and total SO_4^{2-} reducers ($\rho = 0.81$, $p < 0.01$) and the dominant SO_4^{2-} reducing taxa, i.e. *Desulfarculaceae* ($\rho = 0.67$, $p < 0.05$), *Desulfobacterales* ($\rho = 0.64$, $p < 0.05$) and *Desulfobacca* ($\rho = 0.71$, $p < 0.05$,) were coherent at Station 1 (Fig. S2B), where also the highest AOM rates were observed. In contrast, such coherent patterns were not observed for Station 2 and 3. Nevertheless, these results further hint that SO_4^{2-} - mediated AOM takes place in sediments of the study lake.

Although *Methylococcales* are not considered to be anaerobic methanotrophs, they may include species that can couple CH_4 oxidation with reduction of NO_3^-/NO_2^-, Fe^{3+} minerals and organic EAs in hypoxic and anoxic conditions (Kits et al. 2015; Oswald et al. 2016, 2017; Martinez-Cruz et al. 2017; Rissanen et al. 2018; Zheng et al. 2020). As above for methanogens, we could not construct MAGs of *Methylococcales* or any other methanotrophic taxa, probably due to their too low abundance (see Supplementary Results and Table S1). However, according to previous MAG studies, the *Methylococcales* genera that were dominant in the study lake, i.e. *Methylobacter* and *Crenothrix* (60 – 89 % of the 16S rRNA gene amplicons affiliated to *Methylococcales* in the study lake) (Fig. S3), include members that harbored genetic potential for

reduction of Fe^{3+} minerals and organic EAs in the hypoxic and anoxic water column layers of humic lakes, including closely located boreal Lake Lovojärvi (within 4 km from the study lake) (He et al. 2019; Rissanen et al. 2020). Hence, in addition to variation in abundance of *Ca*. Methanoperedens archaea, the higher abundance of *Methylococcales* also supports the observed higher AOM rates at Station 1, potentially coupled with reduction of Fe^{3+} minerals and organic EAs.

The putative NO_2^- reducing AOM-driving bacteria in the genus *Ca*. Methylomirabilis had a higher relative abundance than *Ca*. Methanoperedens archaea at each station (Figs. 3 and 5). Furthermore, their relative abundance was much higher upper in the sediment profile than within the incubation layers especially at Station 2 and 3 (Fig. 3). These results suggest that NO_2^- is an important EA for AOM in the study lake, as shown previously for AOM of various freshwater ecosystems, including lakes (Deutzmann et al. 2014; Welte et al. 2016).

Recent results also suggest that besides ANME archaea, methanogens may drive AOM coupled with electron transfer to solid EAs, e.g. Fe^{3+} minerals (Bar-Or et al. 2017; Yu et al. 2021). However, none of the methanogenic taxa in the AOM incubation layers had a significantly higher relative abundance at Station 1 than at other stations (Fig. S4). Thus, variations in the methanogenic community did not explain the differences in the AOM rates between stations, which suggests that methanogens did not contribute to AOM in the study lake.

Conclusions

According to geochemical profiles as well as experimental incubations, AOM took place in the sediments of the study lake. However, despite geochemical profiles showing simultaneous

consumption of CH_4 and NO_3^- in the depth layers chosen for the experimental incubations, the AOM rates were independent of NO_3^- concentration. These results suggest that AOM may not be directly coupled to nitrate reduction in sediments of nitrate-rich, oligo-mesotrophic, boreal lakes. Instead, the geochemical profiles and the microbiological data both hint towards contribution of Fe^{3+} and SO_4^{2-}, while microbiological data further hint towards contribution of organic EAs and NO_2^- in driving AOM in the sediments of such ecosystems, which needs to be confirmed in future experimental studies.

Funding This study was supported by Academy of Finland (Grant No. 286642 for AJR, 323214 for RM, 307331 for HJ, and 310302 for SLA), joint funding by Olvi Foundation, Jenny and Antti Wihuri Foundation, and Saastamoinen Foundation (for HJ) and Kone Foundation (Grant No. 201803224 for AJR), and a Tenure Track starting package from University of Helsinki (TJ).

Conflicts of interest/Competing interests None declared.

Availability of data and material The sequences of the 16S rRNA gene amplicon dataset are deposited in NCBI´s Sequence Read Archive (SRA) under the accession number PRJNA627335. The sequences of the shotgun metagenomic dataset are deposited in European Nucleotide Archive (ENA) under the accession number PRJEB29513.

Code availability Not applicable

Author´s contributions AJR, HJ and TJ designed the sampling and the experiments. All authors took part in acquisition, analysis and interpretation of the data. AJR drafted the manuscript, while all other authors took part in making substantial revision of the draft. All authors approved the version to be published.

Acknowledgements

We thank staff at the Lammi Biological Station for their support in field and laboratory work.

References

Apprill A, McNally S, Parsons R, Weber L (2015) Minor revision to V4 region SSU rRNA 806R gene primer greatly increases detection of SAR11 bacterioplankton. Aquat Microb Ecol 75:129–137

Arvola L, Kankaala P, Tulonen T, Ojala A (1996) Effects of phosphorus and allochthonous humic matter enrichment on metabolic processes and community structure of plankton in a boreal lake (Lake Pääjärvi). Can J Fish Aquat Sci 53:1646–1662. doi: 10.1139/f96-083

Bai Y-N, Wang X-N, Wu J, et al (2019) Humic substances as electron acceptors for anaerobic oxidation of methane driven by ANME-2d. Water Res 164:114935. doi: https://doi.org/10.1016/j.watres.2019.114935

Bar-Or I, Elvert M, Eckert W, et al (2017) Iron-Coupled Anaerobic Oxidation of Methane Performed by a Mixed Bacterial-Archaeal Community Based on Poorly Reactive Minerals. Environ Sci Technol 51:12293–12301. doi: 10.1021/acs.est.7b03126

Bastviken D, Tranvik LJ, Downing JA, et al (2011) Freshwater methane emissions offset the continental carbon sink. Science 331:50. doi: 10.1126/science.1196808

Beal EJ, House CH, Orphan VJ (2009) Manganese- and iron-dependent marine methane oxidation. Science 325:184–187. doi: 10.1126/science.1169984

Bolger AM, Lohse M, Usadel B (2014) Trimmomatic: a flexible trimmer for Illumina sequence data. Bioinformatics 30:2114–2120. doi: 10.1093/bioinformatics/btu170

Borrel G, O'Toole PW, Harris HM, et al (2013) Phylogenomic data support a seventh order of methylotrophic methanogens and provide insights into the evolution of methanogenesis. Genome Biol Evol 5:1769–80

Conrad R (1999) Contribution of hydrogen to methane production and control of hydrogen concentrations in methanogenic soils and sediments. FEMS Microbiol Ecol 28:193–202. doi: 10.1111/j.1574-6941.1999.tb00575.x

Deutzmann JS, Schink B (2011) Anaerobic oxidation of methane in sediments of Lake Constance, an oligotrophic freshwater lake. Appl Environ Microbiol 77:4429–4436. doi: 10.1128/AEM.00340-11

Deutzmann JS, Stief P, Brandes J, Schink B (2014) Anaerobic methane oxidation coupled to denitrification is the dominant methane sink in a deep lake. Proc Natl Acad Sci U S A 111:18273–18278. doi: 10.1073/pnas.1411617111

Ettwig KF, Butler MK, Le Paslier D, et al (2010) Nitrite-driven anaerobic methane oxidation by oxygenic bacteria. Nature 464:543–548

Ettwig KF, Zhu B, Speth D, et al (2016) Archaea catalyze iron-dependent anaerobic oxidation of methane. Proc Natl Acad Sci 113:12792–12796. doi: 10.1073/pnas.1609534113

Goñi MA, Teixeira MJ, Perkey DW (2003) Sources and distribution of organic matter in a river-dominated estuary (Winyah Bay, SC, USA). Estuar Coast Shelf Sci 57:1023–1048. doi: https://doi.org/10.1016/S0272-7714(03)00008-8

Haroon MF, Hu S, Shi Y, et al (2013) Anaerobic oxidation of methane coupled to nitrate reduction in a novel archaeal lineage. Nature 500:567–570

He S, Lau MP, Linz AM, et al (2019) Extracellular Electron Transfer May Be an Overlooked Contribution to Pelagic Respiration in Humic-Rich Freshwater Lakes. mSphere 4:e00436-18. doi: 10.1128/mSphere.00436-18

Iino T, Tamaki H, Tamazawa S, et al (2013) Candidatus Methanogranum caenicola: a novel methanogen from the anaerobic digested sludge, and proposal of methanomassiliicoccaceae fam. nov. and Methanomassiliicoccales ord. nov., for a Methanogenic Lineage of the Class Thermoplasmata. Microbes Environ 28:244-250

Jilbert T, Asmala E, Schröder C, et al (2018) Impacts of flocculation on the distribution and diagenesis of iron in boreal estuarine sediments. Biogeosciences 15:1243–1271. doi: 10.5194/bg-15-1243-2018

Jilbert T, Jokinen S, Saarinen T, et al (2020) Impacts of a deep reactive layer on sedimentary phosphorus dynamics in a boreal lake recovering from eutrophication. Hydrobiologia 847:4401–4423. doi: 10.1007/s10750-020-04289-9

Kallistova A, Kadnikov V, Rusanov I, et al (2018) Microbial communities involved in aerobic and anaerobic methane cycling in a meromictic ferruginous subarctic lake. Aquat Microb Ecol 82:1–18

Kang D., Froula J, Egan R, Wang Z (2015) MetaBAT, an efficient tool for accurately reconstructing single genomes from complex microbial communities. PeerJ 3:e1165

Kang D., Li F, Kirton E, et al (2019) MetaBAT 2: an adaptive binning algorithm for robust and efficient genome reconstruction from metagenome assemblies. PeerJ 7:e7359

Kits KD, Klotz MG, Stein LY (2015) Methane oxidation coupled to nitrate reduction under hypoxia by the Gammaproteobacterium Methylomonas denitrificans, sp. nov. type strain FJG1. Environ Microbiol 17:3219–3232. doi: 10.1111/1462-2920.12772

Knittel K, Boetius A (2009) Anaerobic oxidation of methane: progress with an unknown process. Annu Rev Microbiol 63:311–334. doi: 10.1146/annurev.micro.61.080706.093130

Kortelainen P, Pajunen H, Rantakari M, Saarnisto M (2004) A large carbon pool and small sink in boreal Holocene lake sediments. Glob Chang Biol 10:1648–1653. doi: https://doi.org/10.1111/j.1365-2486.2004.00848.x

Kortelainen P, Saukkonen S (1995) Organic vs. minerogenic acidity in headwater streams in

Finland. Water Air Soil Pollut 85:559–564. doi: 10.1007/BF00476888

Li D, Liu C-M, Luo R, et al (2015) MEGAHIT: an ultra-fast single-node solution for large and complex metagenomics assembly via succinct de Bruijn graph. Bioinformatics 31:1674–1676. doi: 10.1093/bioinformatics/btv033

Martinez-Cruz K, Leewis M-C, Herriott IC, et al (2017) Anaerobic oxidation of methane by aerobic methanotrophs in sub-Arctic lake sediments. Sci Total Environ 607:23–31. doi: http://dx.doi.org/10.1016/j.scitotenv.2017.06.187

Martinez-Cruz K, Sepulveda-Jauregui A, Casper P, et al (2018) Ubiquitous and significant anaerobic oxidation of methane in freshwater lake sediments. Water Res 144:332–340. doi: https://doi.org/10.1016/j.watres.2018.07.053

Menzel P, Ng KL, Krogh A (2016) Fast and sensitive taxonomic classification for metagenomics with Kaiju. Nat Commun 7:11257. doi: 10.1038/ncomms11257

Miranda KM, Espey MG, Wink DA (2001) A Rapid, Simple Spectrophotometric Method for Simultaneous Detection of Nitrate and Nitrite. Nitric Oxide 5:62–71. doi: https://doi.org/10.1006/niox.2000.0319

Mitchell AL, Scheremetjew M, Denise H, et al (2017) EBI Metagenomics in 2017: enriching the analysis of microbial communities, from sequence reads to assemblies. Nucleic Acids Res 46:D726–D735. doi: 10.1093/nar/gkx967

Myllykangas J-P, Rissanen AJ, Hietanen S, Jilbert T (2020) Influence of electron acceptor availability and microbial community structure on sedimentary methane oxidation in a boreal estuary. Biogeochemistry 148:291–309. doi: 10.1007/s10533-020-00660-z

Nazaries L, Murrell JC, Millard P, et al (2013) Methane, microbes and models: fundamental understanding of the soil methane cycle for future predictions. Environ Microbiol 15:2395–2417. doi: 10.1111/1462-2920.12149

Norði K á., Thamdrup B (2014) Nitrate-dependent anaerobic methane oxidation in a freshwater sediment. Geochim Cosmochim Acta 132:141–150. doi: http://dx.doi.org/10.1016/j.gca.2014.01.032

Oswald K, Graf JS, Littmann S, et al (2017) Crenothrix are major methane consumers in stratified lakes. Isme J 11:2124

Oswald K, Milucka J, Brand A, et al (2016) Aerobic gammaproteobacterial methanotrophs mitigate methane emissions from oxic and anoxic lake waters. Limnol Oceanogr 61:S101–S118. doi: 10.1002/lno.10312

Pajunen H (2000) Carbon in Finnish lake sediments. Geological Survey of Finland, Espoo, Finland

Parada AE, Needham DM, Fuhrman JA (2016) Every base matters: assessing small subunit rRNA primers for marine microbiomes with mock communities, time series and global field samples. Environ Microbiol 18:1403–1414. doi: 10.1111/1462-2920.13023

Parks DH, Imelfort M, Skennerton CT, et al (2015) CheckM: assessing the quality of microbial

genomes recovered from isolates, single cells, and metagenomes. Genome Res 25:1043–1055. doi: 10.1101/gr.186072.114

Rissanen AJ, Karvinen A, Nykänen H, et al (2017) Effects of alternative electron acceptors on the activity and community structure of methane-producing and consuming microbes in the sediments of two shallow boreal lakes. FEMS Microbiol Ecol 93:fix078

Rissanen AJ, Saarela T, Jäntti H, et al (2020) Vertical stratification patterns of methanotrophs and their genetic controllers in water columns of oxygen-stratified boreal lakes. FEMS Microbiol Ecol. doi: 10.1093/femsec/fiaa252

Rissanen AJ, Saarenheimo J, Tiirola M, et al (2018) Gammaproteobacterial methanotrophs dominate methanotrophy in aerobic and anaerobic layers of boreal lake waters. Aquat Microb Ecol 81:257–276. doi: https://doi.org/10.3354/ame01874

Salmela M, Lehtinen T, Efimova E, et al (2018) Metabolic pairing of aerobic and anaerobic production in a one-pot batch cultivation. Biotechnol Biofuels 11:187 doi: 10.1186/s13068-018-1186-9

Salonen K (1981) The ecosystem of the oligotrophic Lake Pääjärvi 2. Bacterioplankton. Verh Internat Verein Limnol 21:448–453. doi: 10.1080/03680770.1980.11897021

Saunois M, Stavert AR, Poulter B, et al (2020) The Global Methane Budget 2000–2017. Earth Syst Sci Data 12:1561–1623. doi: 10.5194/essd-12-1561-2020

Seemann T (2014) Prokka: rapid prokaryotic genome annotation. Bioinformatics 30:2068–2069. doi: 10.1093/bioinformatics/btu153

Speth D, Orphan V (2018) Metabolic marker gene mining provides insight in global mcrA diversity and, coupled with targeted genome reconstruction, sheds further light on metabolic potential of the Methanomassiliicoccales. PeerJ 6:e5614

Su G, Zopfi J, Yao H, et al (2019) Manganese/iron-supported sulfate-dependent anaerobic oxidation of methane by archaea in lake sediments. Limnol Oceanogr 65:863-875. doi: 10.1002/lno.11354

Timmers PHA, Welte CU, Koehorst JJ, et al (2017) Reverse Methanogenesis and Respiration in Methanotrophic Archaea. Archaea 2017: Article ID 1654237

Valenzuela EI, Prieto-Davó A, López-Lozano NE, et al (2017) Anaerobic Methane Oxidation Driven by Microbial Reduction of Natural Organic Matter in a Tropical Wetland. Appl Environ Microbiol 83:e00645-17. doi: 10.1128/AEM.00645-17

von Meijenfeldt FAB, Arkhipova K, Cambuy DD, et al (2019) Robust taxonomic classification of uncharted microbial sequences and bins with CAT and BAT. Genome Biol 20:217. doi: 10.1186/s13059-019-1817-x

Weber HS, Habicht KS, Thamdrup B (2017) Anaerobic Methanotrophic Archaea of the ANME-2d Cluster Are Active in a Low-sulfate, Iron-rich Freshwater Sediment. Front. Microbiol. 8:619

Welte CU, Rasigraf O, Vaksmaa A, et al (2016) Nitrate- and nitrite-dependent anaerobic

oxidation of methane. Environ. Microbiol. Rep. 8:941–955

Wik M, Varner RK, Anthony KW, et al (2016) Climate-sensitive northern lakes and ponds are critical components of methane release. Nat Geosci 9:99–105

Wood ED, Armstrong FAJ, Richards FA (1967) Determination of nitrate in sea water by cadmium-copper reduction to nitrite. J Mar Biol Assoc United Kingdom 47:23–31. doi: 10.1017/S002531540003352X

Yu L, He D, Zhang E, et al (2021) Electricity from anaerobic methane oxidation by a single methanogenic archaeon Methanosarcina barkeri. Chem Eng J 405:126691. doi: https://doi.org/10.1016/j.cej.2020.126691

Zheng Y, Wang H, Liu Y, et al (2020) Methane-Dependent Mineral Reduction by Aerobic Methanotrophs under Hypoxia. Environ Sci Technol Lett 7:606–612. doi: 10.1021/acs.estlett.0c00436

Table 1 Station coordinates, depth, temperature and O_2 concentration measured approximately 50 cm above the sediment surface and NO_3^- concentrations measured 5 cm above the sediment. Loss on ignition (LOI) was measured from the top 0.5 cm of the sediment

Station	N	E	Depth (m)	Temp (°C)	O_2 (µmol L^{-1})	NO_3^- (µmol L^{-1})	LOI (%)
1	61.03.046	25.03.606	14	9.3	254	60.0	14.6
2	61.03.192	25.05.449	22	6.4	314	62.0	13.4
3	61.03.487	25.06.163	52	5.4	303	45.5	14.2

Fig. 1

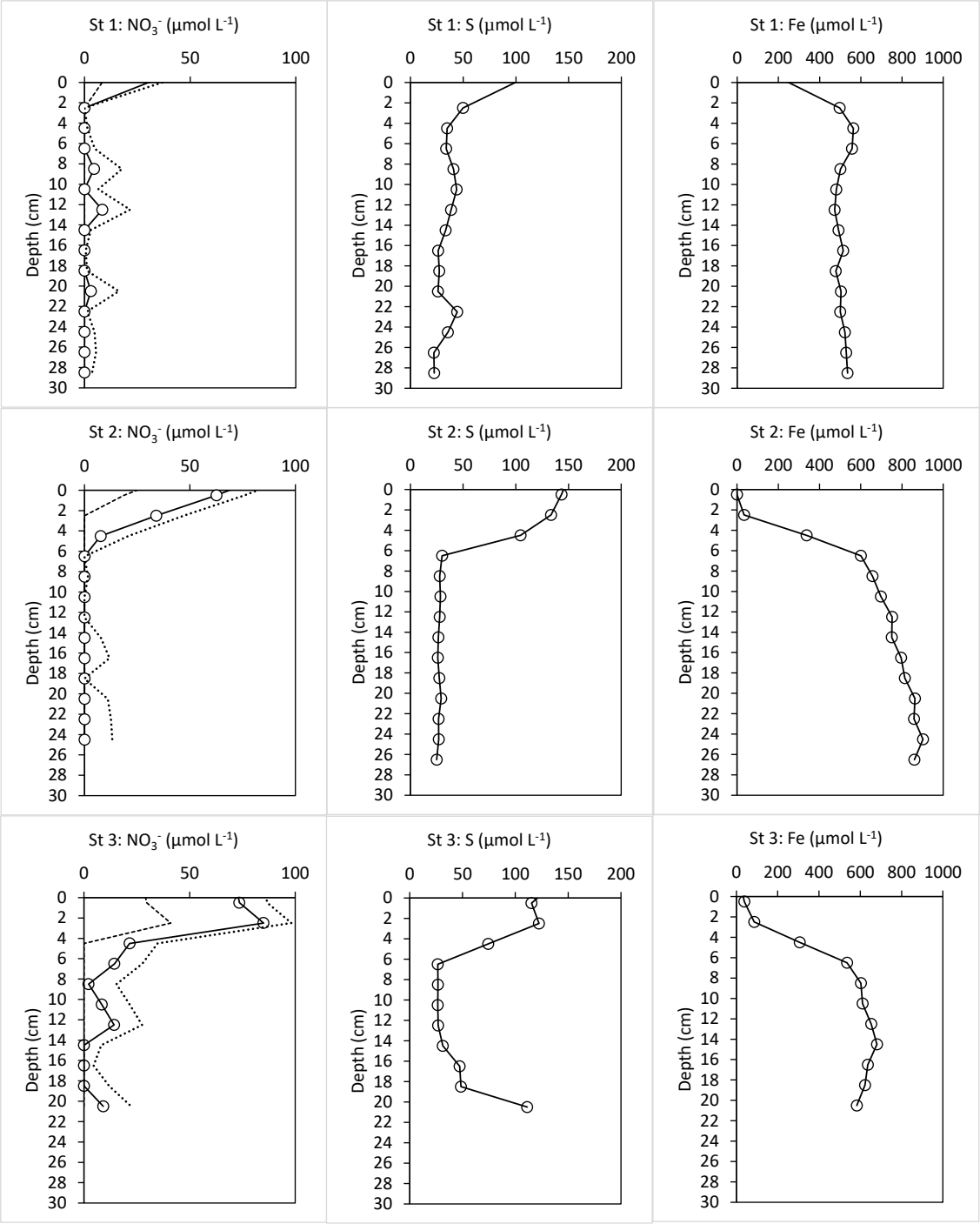

Fig. 1. Sediment porewater profiles of dissolved NO_3^- (left panels), S (middle panels) and Fe (right panels) at Stations 1 (upper panels), 2 (middle panels) and 3 (lower panels). The extent of the NO_3^- contamination resulting from HNO_3 washing of porewater samplers was tested and the NO_3^- data is presented as values from which average (solid line with symbols), minimum and maximum contamination (dotted lines) was subtracted (see Materials and Methods). To allow comparison with the microbiological data, the profiles are specifically shown for the top 10 cm layer also in Fig. 3

Fig. 2

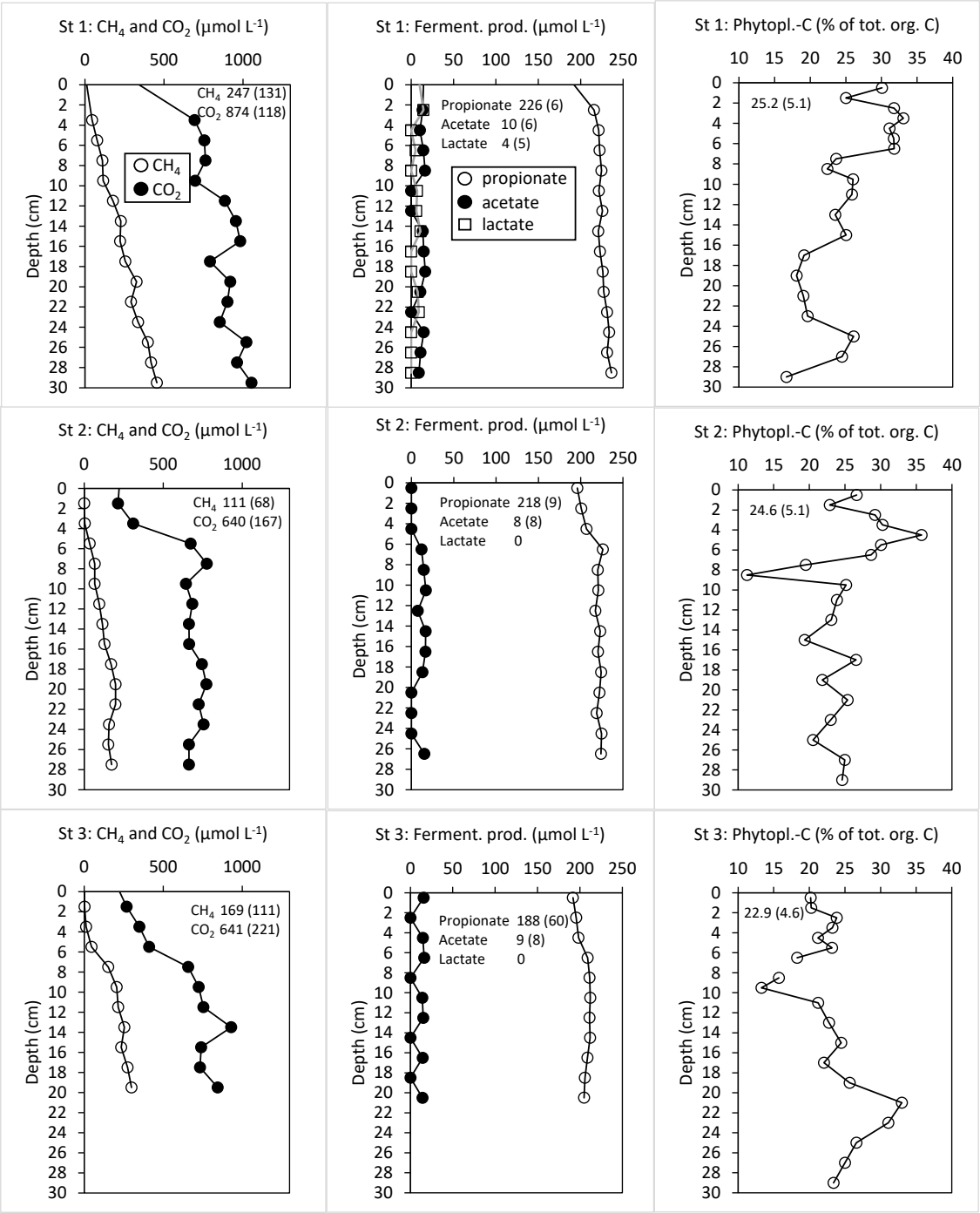

Fig. 2. Profiles of CH_4 and CO_2 (left panels), organic fermentation products (middle panels) and estimated contribution of labile phytoplankton-derived organic carbon in total organic carbon in sediments (right panels) at Stations 1 (upper panels), 2 (middle panels) and 3 (lower panels). Average values (±SD) calculated across the profiles for each variable are shown within the figures. To allow comparison with the microbiological data, the profile of CH_4 is specifically shown for the top 10 cm layer also in Fig. 3

Fig. 3

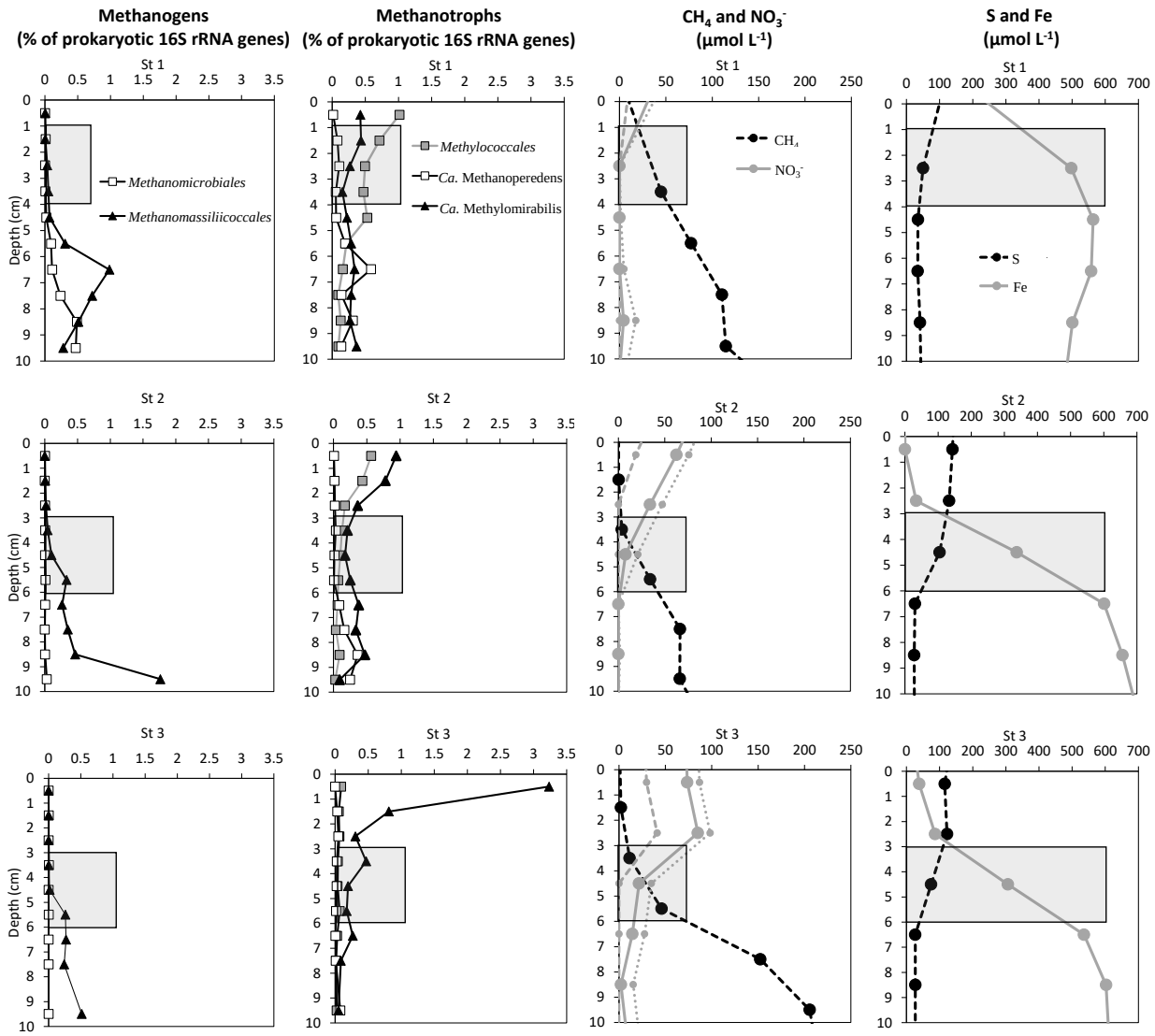

Fig. 3. Vertical depth profiles of methanogens (left panels) and methanotrophs (second left panels) based on 16S rRNA gene amplicon sequencing, as well as CH_4, NO_3^- (second right panels), S and Fe (right panels) in the topmost 10 cm of sediments at Stations 1 (upper panels), 2 (middle panels) and 3 (lower panels). The layers chosen for AOM incubation analyses are highlighted with grey color. See Fig. 1 for explanation on the presentation of the NO_3^- data

Fig. 4

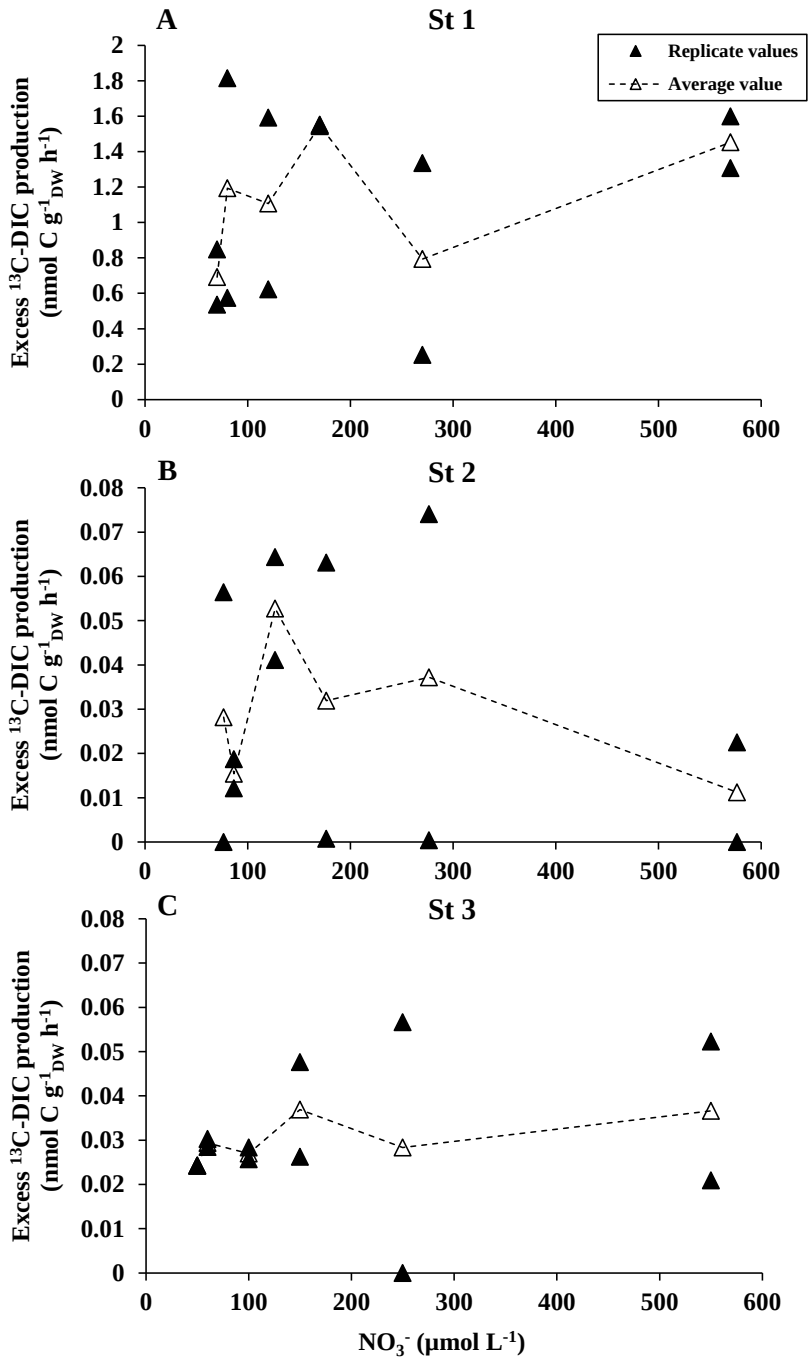

Fig. 4. AOM rate, i.e. production of excess ^{13}C-DIC, at different concentrations of NO_3^- at **A** Station 1, **B** Station 2 and **C** Station 3. Values are represented as replicate and average values (n=2 at each concentration level of NO_3^-). The NO_3^- concentration levels at the x-axis represent the sum of added NO_3^- (i.e. 0, 10, 50, 100, 200 or 500 µmol L^{-1}) and NO_3^- already present in slurry at the beginning of incubations (i.e. 70, 77 and 50 µmol L^{-1} for stations 1, 2 and 3, respectively). No positive relationship between NO_3^- and AOM was observed at the stations. Note different scale in y-axis in **A** compared to **B** and **C**

Fig. 5

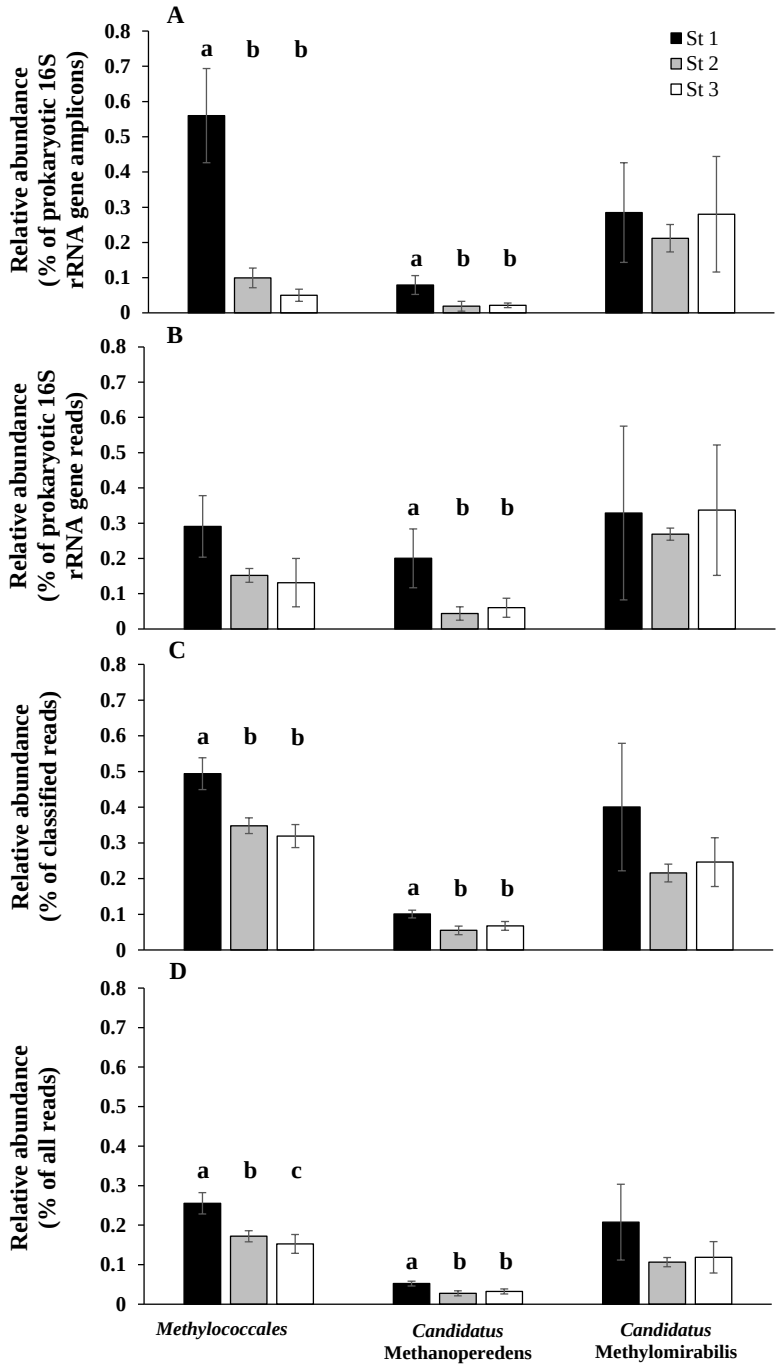

Fig. 5. Relative abundance of different methanotrophic taxa in the depth layers representing the incubation layers based on **A** 16S rRNA gene amplicon sequencing, as well as **B**-**D** shotgun metagenomic sequencing, i.e **B** 16S rRNA gene reads, **C** KAIJU-classified reads expressed as relative to reads that were classified at least to domain-level and **D** KAIJU-classified reads expressed as relative to all reads. Data is represented as an average and standard deviation of three layer-specific samples. Different letters above bars indicate significant differences in RB-ANOVA and subsequent pairwise tests ($p < 0.05$)